5-1-2007

Experimental Evidence for a Metallohydrolase Mechanism in Which the Nucleophile Is Not Delivered by a Metal Ion: EPR Spectrokinetic and Structural Studies of Aminopeptidase from *Vibrio proteolyticus*

Amit Kumar
Medical College of Wisconsin

Gopal R. Periyannan
Eastern Illinois University

Aaron W. Kittell
Medical College of Wisconsin

Jung Ja Kim
Medical College of Wisconsin

Brian Bennett
Marquette University, brian.bennett@marquette.edu

Accepted version. *Biochemical Journal*, Vol. 403, No. 3 (May 1, 2007): 527-536. DOI. The final version of record is available at http://dx.doi.org/10.1042/BJ20061591.
Brian Bennett was affiliated with the Medical College of Wisconsin at the time of publication.

Experimental Evidence for A Metallohydrolase Mechanism In Which The Nucleophile Is Not Delivered By A Metal Ion: EPR Spectrokinetic And Structural Studies Of Aminopeptidase from *Vibrio proteolyticus*

Amit Kumar
Department of Biophysics, Medical College of Wisconsin, Milwaukee, WI
Gopal Raj Periyannan
Department of Biophysics, Medical College of Wisconsin, Milwaukee, WI
Beena Narayanan
Department of Biochemistry, Medical College of Wisconsin, Milwaukee, WI
Aaron W. Kittell
Department of Biophysics, Medical College of Wisconsin, Milwaukee, WI
Jung-Ja Kim
Department of Biochemistry, Medical College of Wisconsin, Milwaukee, WI

Biochemical Journal, Vol. 403, No. 3 (May 1, 2007): pg. 527-536. DOI.

Brian Bennett

Department of Biophysics, Medical College of Wisconsin, Milwaukee, WI

Abstract

Metallohydrolases catalyse some of the most important reactions in biology and are targets for numerous chemotherapeutic agents designed to combat bacterial infectivity, antibiotic resistance, HIV infectivity, tumour growth, angiogenesis and immune disorders. Rational design of inhibitors of these enzymes with chemotherapeutic potential relies on detailed knowledge of the catalytic mechanism. The roles of the catalytic transition ions in these enzymes have long been assumed to include the activation and delivery of a nucleophilic hydroxy moiety. In the present study, catalytic intermediates in the hydrolysis of L-leucyl-L-leucyl-L-leucine by *Vibrio proteolyticus* aminopeptidase were characterized in spectrokinetic and structural studies. Rapid-freeze-quench EPR studies of reaction products of L-leucyl-L-leucyl-L-leucine and Co(II)-substituted aminopeptidase, and comparison of the EPR data with those from structurally characterized complexes of aminopeptidase with inhibitors, indicated the formation of a catalytically competent post-Michaelis pre-transition state intermediate with a structure analogous to that of the inhibited complex with bestatin. The X-ray crystal structure of an aminopeptidase–L-leucyl-L-leucyl-L-leucine complex was also analogous to that of the bestatin complex. In these structures, no water/hydroxy group was observed bound to the essential metal ion. However, a water/hydroxy group was clearly identified that was bound to the metal-ligating oxygen atom of Glu^{152}. This water/hydroxy group is proposed as a candidate for the active nucleophile in a novel metallohydrolase mechanism that shares features of the catalytic mechanisms of aspartic proteases and of B2 metallo-β-lactamases. Preliminary studies on site-directed variants are consistent with the proposal. Other features of the structure suggest roles for the dinuclear centre in geometrically and electrophilically activating the substrate.

Keywords: aminopeptidase, cobalt, EPR, metallohydrolase, *Vibrio proteolyticus*, zinc

Abbreviations: BuBA, 1-butaneboronic acid; LL, L-leucyl-L-leucine; LLL, L-leucyl-L-leucyl-L-leucine; LPA, L-leucine phosphonic acid; LPNA, L-leucine-*p*-nitroanilide; PSMA, prostate-specific membrane antigen; RFQ, rapid-freeze-quench; VpAP, aminopeptidase from *Vibrio proteolyticus*

Biochemical Journal, Vol. 403, No. 3 (May 1, 2007): pg. 527-536. DOI.

Introduction

The aminopeptidase from the bacterium *Vibrio proteolyticus* (VpAP) is one of the more intensively studied metalloaminopeptidases [1,2]. Metalloaminopeptidases are key players in cellular targeting of proteins and protein degradation [3,4], aging [5], cataract formation [6], HIV infectivity [7], bacterial infectivity [8], angiogenesis [9,10] and cancer [9,11]. VpAP itself is of significant biomedical interest on two accounts. First, aminopeptidases that are almost identical with VpAP and are secreted by pathogenic bacteria that include species of *Vibrio*, *Aeromonas*, *Streptomyces* and *Clostridium* have been shown to be virulence factors in infectivity [8,12,13]. Aeromonad and non-choleraic vibrioid infections are an emerging public health concern, giving rise to meningitis, osteomyelitis (bone infection), endocarditis (infection of the lining and valves of the heart), wound infection and, particularly, gastroenteritis [14–17]. Many of these bacteria have now been found to have developed resistance to both traditional and 'third-generation' antibiotics [18], but appear to be sensitive to metalloaminopeptidase inhibitors [19]. VpAP inhibitors are therefore possible candidates or templates for antibacterial drugs. A second reason for interest in VpAP is the association of leucine aminopeptidase activity with some cancers and the antitumour efficacy of some potent VpAP inhibitors [7,20]. In addition, a THREADER [21] analysis predicted that VpAP would have a strong (P=1) structural homology with the carboxypeptidatic domain of the PSMA (prostate-specific membrane antigen); this has been confirmed following crystallographic characterization of the PSMA ectodomain, and the dimetallic active sites of these enzymes are superimposable [22]. Thus mechanistic information on VpAP may well be relevant to PSMA and other peptidases involved in cancer.

Native VpAP contains a (μ-aquo)(μ-carboxylato)-bridged dizinc active site [23]. Zn(II) can be site-specifically replaced in either the first ('M1') or second ('M2') site by many other transition ions, and Co(II) furnishes monometallic [Co_(VpAP)], homodimetallic [CoCo(VpAP)] and heterodimetallic [CoZn(VpAP)] and [ZnCo(VpAP)] forms of the enzyme that, functionally, closely resemble the native zinc-containing enzyme [24–26]. A combination of EPR spectroscopy of Co(II)-containing VpAP and X-ray crystallography has been used to

Biochemical Journal, Vol. 403, No. 3 (May 1, 2007): pg. 527-536. DOI.

characterize the resting state, an inhibited species corresponding to a putative Michaelis complex analogue, and a transition state analogue complex of the enzyme [24,25,27–31]. Kinetic studies have provided further mechanistic insight [26,32]. A detailed mechanism has been proposed on the basis of these studies and was presented in graphic form as Figure 10 in the original description by Petsko, Holz and co-workers [31]. The mechanism invokes (i) binding of substrate to a substrate-recognition site distinct from the metal-containing active site, (ii) binding of the carbonyl oxygen of the substrate to the M1 metal ion, with concomitant terminalization of the hitherto bridging water molecule, providing an activated nucleophilic hydroxy group, also bound to M1, (iii) nucleophilic attack of the M1-bound nucleophile at the carbonyl carbon atom, forming a tetrahedral transition state, and (iv) collapse of the transition state and proton transfer from Glu^{151}, yielding product and resting enzyme. Consistent with this proposed mechanism, M1 is essential for catalysis. In contrast, the effect of the presence of the second, M2, metal ion on catalytic parameters is complex and is dependent on the nature of both M1 and M2. EPR and crystallographic studies with the transition-state analogue inhibitor LPA (L-leucine phosphonic acid) have characterized strong interactions between LPA and the M2 metal ion, and M2 was proposed to function to stabilize the transition state. Thus the primary function of M1 has been described as providing the hydrolytic nucleophile for attack on the M1-immobilized substrate, whereas that of M2 is to stabilize the transition state.

In order to obtain further information on the hydrolytic mechanism of VpAP, we carried out EPR spectrokinetic and X-ray crystallographic studies of the enzyme using the *bona fide* substrate LLL (L-leucyl-L-leucyl-L-leucine). While the proposed mechanism for VpAP is consistent with a substantial body of experimental work, other observations do not sit well with it. The complex substrate specificity of VpAP and very closely related enzymes [33–37], the reaction specificity, and the unusual and complex pattern of activation by transition ions [26,38] are not explained by the proposed roles of M1 in the exposed active site of VpAP. The difficulty of reconciling these and other observations with the proposed hydrolytic mechanism of VpAP prompted a reexamination of the mechanism. For the first time, direct structural information on the reaction of *bona fide* substrates with VpAP was sought. In the present work, we describe the EPR

Biochemical Journal, Vol. 403, No. 3 (May 1, 2007): pg. 527-536. DOI.

spectra of catalytic intermediate species generated by RFQ (rapid-freeze-quench) techniques and the X-ray crystallographic structure of VpAP in complex with the substrate LLL. Comparison of the EPR and structural data with X-ray crystallographic structures and EPR data from VpAP complexes with the inhibitors bestatin {ubenimex; *N*-[(2*S*,3*R*)-3-amino-2-hydroxy-4-phenyl-butyryl]-L-leucine} and amastatin {(2*S*,3*R*)-3-amino-2-hydroxy-5-methylhexanoyl-Val-Val-Asp-OH} indicate that the active site of the VpAP–LLL complex characterized by X-ray crystallography corresponds to a catalytically competent species in solution and observed in the RFQ–EPR studies. On the basis of these data, a hitherto unconsidered novel mechanism is proposed for the N-terminal hydrolysis of LLL by VpAP. The proposed mechanism contains aspects of those of aspartic proteases and class II aldolases, and of the mechanism recently proposed for the class B2 metallo-β-lactamases on the basis of computational studies [39]. This mechanism may represent a new paradigm for metalloenzyme-catalysed hydrolysis in what could be considered a distinct class of metallohydrolases, one in which the hydrolytically active nucleophile is not delivered to the substrate by the metal ion(s).

Experimental

General chemicals

Except where stated, all reagents were of ACS or equivalent quality. Milli-Q purified water (Millipore) was used throughout. Sea salt, for culture of *V. proteolyticus*, was obtained from Sigma–Aldrich. 2-Methylbutane (isopentane) used for RFQ was certified ≥95% grade from Fisher.

VpAP preparation

VpAP was purified from the supernatant of a 10 litre fermenter (BioFlo) culture of *V. proteolyticus* (obtained from Professor R.C. Holz, Department of Chemistry and Biochemistry, Utah State University, Logan, UT, U.S.A.) as described in previous work [24]. VpAP was characterized by electronic absorption spectrophotometry [40], hydrolytic activity towards LPNA (L-leucine-*p*-nitroanilide) [26], SDS/PAGE (12% gels) [41] and the Bio-Rad protein-binding dye assay

Biochemical Journal, Vol. 403, No. 3 (May 1, 2007): pg. 527-536. DOI.

[42] using well-characterized samples of purified VpAP as standards. VpAP thus characterized was found to be >95% pure by SDS/PAGE (12% gels), with specific activity indistinguishable from earlier preparations. ApoVpAP was prepared by dialysis against 1,10-phenanthroline for 72 h at 4 °C, followed by exhaustive dialysis against Chelex™-treated buffer (50 mM Hepes, pH 7.2). [Co_(VpAP)] was prepared by the addition of 1 equiv. of $CoCl_2$, and [CoZn(VpAP)] was prepared by incubation with 0.9 equiv. of $CoCl_2$ for 10 min at 25 °C, followed by addition of 1.1 equiv. of $ZnCl_2$.

Site-directed variants of VpAP

Recombinant wild-type and site-directed variants of VpAP were generated using the expression system of Bzymek and Holz [32] and Bzymek et al. [43]. Expression was induced in cell cultures exhibiting a D_{600} of ~0.9 with 1 mM IPTG (isopropyl β-D-thiogalactoside) and the cultures were incubated further at 30 °C for 5.5 h with agitation in air at 250 rev./min. Supernatant was clarified by centrifugation at 6500 ***g*** for 10 min, and VpAP was precipitated with 560 g/l $(NH_4)_2SO_4$. The precipitate was pelleted at 10500 ***g*** for 1 h, redissolved in 50 mM Hepes buffer, pH 7.5, dialysed against Hepes buffer, treated with proteinase K and heat-treated for 2 h at 70 °C to denature contaminating proteins and to process the translated polypeptide to the mature enzyme form [43].

Kinetic studies

Hydrolysis of LPNA, LL (L-leucyl-L-leucine) and LLL was monitored spectrophotometrically at 405 and 220 nm respectively using an Applied Photophysics Model SX.18MV stopped-flow instrument at 2–40 °C. LLL, LL or LPNA (2.5 mM final concentration) was reacted with VpAP (27.5 μM final concentration) in 10 mM Tricine buffer, pH 8.0. Apparent kinetic parameters K'_m and k'_{cat} for hydrolysis of LLL to LL, LL to leucine, and LPNA to leucine and *p*-nitroanilide under these conditions were estimated by fitting the appropriate part of the progress curve that exhibited a linear relationship between $t^{-1}\{\ln([S_0]/[S_t])\}$ and $t^{-1}([S_0]-[S_t])$ [44].

Biochemical Journal, Vol. 403, No. 3 (May 1, 2007): pg. 527-536. DOI.

RFQ–EPR studies

RFQ was carried out using the apparatus described in detail and calibrated as in previous studies [45]. LLL (2.5 mM final concentration) was reacted with 0.5 mM (final concentration) [CoZn(VpAP)] for 10 ms–1 s at 2 °C. A sample was thawed and refrozen and was estimated to have been incubated for 1 min. [CoZn(VpAP)] has been reported to exhibit a pH-dependent mixture of EPR signals, a rhombic signal with ^{59}Co hyperfine splitting and an axial signal devoid of hyperfine structure [24,25]. It was observed that this form of VpAP exhibited an essentially pure rhombic signal following incubation with substrate (LPNA or LLL) and recovery by dialysis, and this form of the enzyme was used as the starting material for RFQ–EPR studies. EPR was performed using a Bruker E500 EleXsys spectrometer equipped with an ER4116DM TE_{012}/TE_{021} dual mode cavity operating at 9.63 GHz in normal ($B_{static} \| B_{microwave}$) mode. Temperature control was effected using an Oxford Instruments ESR900 helium flow cryostat and ITC502 temperature controller. Spectra were recorded at 9 K and 2 mW microwave power, with 1.06 mT (10.6 G) field modulation at 100 kHz. These conditions provided the best signal-to-noise ratio attainable without detectable distortion of the spectra due to saturation, relaxation broadening or rapid-passage effects. Individual EPR-detectable species were isolated by difference analysis of spectra of resting enzyme and of reaction mixtures trapped at various times. Basis spectra were confirmed as single species by computer simulation (XSophe, Bruker Biospin [46]). Experimental spectra were modelled, and contributions of individual species were quantified, by linear combination and double integration respectively, of simulated basis spectra. The reference sample for quantification was 0.5 mM Co(II) in 50 mM Hepes buffer, pH 7.2, and 50% glycerol, recorded under non-saturating conditions (0.1 mW, 13 K), and the standard corrections for $g_{x(\text{eff.})}$av., 1/T and (microwave power)$^{1/2}$ were applied.

Crystallization of VpAP

VpAP was crystallized using the sitting-drop method. VpAP (0.5 mM) in 10 mM Tris buffer, pH 8.0, containing 10 mM KSCN and 400 mM NaCl was equilibrated with 100 mM Tris buffer, pH 8.0, containing 100 mM KSCN and 4.5 M NaCl; Tris was found to be an

Biochemical Journal, Vol. 403, No. 3 (May 1, 2007): pg. 527-536. DOI.

essential component. Crystals thus obtained underwent successive transfer and incubation in 100 mM Hepes buffer, pH 8.0, containing 100 mM KSCN and 4.5 M NaCl, in order to remove Tris bound at the active site [47]. A single microcrystalline speck of LLL was added, and the crystallization plate was incubated at 23 °C for 16 h before data collection.

X-ray crystallography

Paratone-N (Hampton Research) was used as a cryoprotectant. The diffraction data were collected at −160 °C on a Rigaku R-AXIS IV++, using Crystal Clear software. One crystal was used to collect the entire set of data. An oscillation step size of 0.5° was used to collect 5.5 min exposures. Data were processed, and unit cell parameters were determined with HKL2000 [48]. Since the aminopeptidase crystal soaked in LLL was isomorphous with that of aminopeptidase bound to BuBA (1-butaneboronic acid), the phases from that structure (PDB code 1CP6 [29]) were used to solve the structure by molecular replacement using AMoRe [49]. Model building was performed with the interactive three-dimensional graphic program, Turbo-Frodo (version OpenGL). The structure was manually inspected with electron density maps with $2F_{obs}-F_{calc}$ and $F_{obs}-F_{calc}$ coefficients. Structures were refined using iterative cycles of energy minimization using the program package CNS1.1 [50], alternating with manual map-fitting and model rebuilding. Progress of the refinement was confirmed by the steady decrease in both the $R_{crystal}$ and R_{free} values. Water molecules were added to the model using the WATERPICK protocol from CNS1.1. Procheck was used to check Ramachandran (Φ, ψ) values [51].

Results

Kinetic studies

As prepared VpAP, and VpAP redissolved from crystalline material, was found to be active towards both LPNA and LLL. A linear relationship between $\ln(k'_{cat})$ and $1/T$ was observed for the hydrolysis of LPNA by VpAP between 6 and 65 °C; the activation energy, E_a, was estimated as 66 kJ·mol^{-1} and apparent kinetic constants for LPNA were K'_m (LPNA)=16 μM (6 °C) and 29 μM (25 °C), and k'_{cat} (LPNA)=13 s^{-1}

Biochemical Journal, Vol. 403, No. 3 (May 1, 2007): pg. 527-536. DOI.

(6 °C) and 82 s^{-1} (25 °C). These data extrapolated to a turnover time of 83 ms at 2 °C. Apparent kinetic constants for LLL and LL, K'_m (LLL)=15 μM (6 °C) and 28 μM (25 °C), k'_{cat} (LLL)=1.7 s^{-1} (6 °C) and 7 s^{-1} (25 °C), K'_m (LL)=48 μM (6 °C) and 90 μM (25 °C), and k'_{cat} (LL)=0.3 s^{-1} (6 °C) and 2.6 s^{-1} (25 °C), indicated similar thermodynamics for these substrates, although with slightly higher values for E_a and, consequently, for the enthalpy of hydrolysis of these substrates. Extrapolated turnover times for LLL and LL at 2 °C were estimated as 380 ms and 3.6 s respectively. Recombinant wild-type VpAP exhibited k'_{cat} (LPNA)=10±3 s^{-1} (25 °C). Of the site-directed variants E152D, E152T, E152S and E152Y, E152D preparations exhibited 30–90% of the specific activity of wild-type VpAP, whereas the others exhibited no activity under the assay conditions used (<5% of wild-type activity). Control preparations from non-transfected cells and from non-induced cultures of wild-type and E151D expression systems did not exhibit any detectable activity towards LPNA.

RFQ–EPR studies

EPR spectra of resting [CoZn(VpAP)] and VpAP reacted with LLL for 10 ms, 20 ms, 1 s and 1 min are shown as traces A–E in Figures 1 and and22 (Figure 2 shows the ^{59}Co hyperfine structure expanded). The spectrum of VpAP before reaction consisted of a single species and was simulated as a rhombic signal with spin Hamiltonian parameters $S=^3/_2$, $M_S=|\pm½\rangle$, $g_{x,y}=2.57$, $g_z=2.24$, $D \gg g\beta BS$ (where $D \gg g\beta BS$, spectra are insensitive to D; D=50 cm^{-1} was used throughout), $E/D=0.21$ and $A_y^{I=7/2}(^{59}Co)=8.1\times10^{-3}$ cm^{-1}. This EPR species is termed the 'resting' species, even where observed in samples other than resting enzyme. Upon reaction with LLL, clear changes in the spectrum were observed and two new species (traces F and G in Figure 1) were isolated from the experimental spectra of Figure 1, traces A, B and C. The spectrum of traces F in Figure 1, termed here the 'LLL-axial' signal, was very broad, no hyperfine structure was resolved, and the high-field g_z feature was not resolved. The LLL-axial signal was consistent with the approximate spin Hamiltonian parameters $g_{x,y}\sim2.28$ and $E/D\sim0$ (the parameters used for simulation were $S=^3/_2$, $M_S=|\pm½\rangle$, $g_{x,y}=2.28$, $g_z=2.20$, D=50 cm^{-1} and $E/D=0.05$). The second species isolated by difference is shown as traces G in Figure 1 and is termed the 'LLL-rhombic' species; simulation returned the spin

Biochemical Journal, Vol. 403, No. 3 (May 1, 2007): pg. 527-536. DOI.

Hamiltonian parameters $S=^3/_2$, $M_S=|\pm½\rangle$, $g_{x,y}=2.56$, $g_z=2.50$, $D \gg g\beta BS$ (50 cm^{-1}), $E/D=0.29$ and $A_y^{I=7/2}(^{59}Co)=8.4\times10^{-3}$ cm^{-1}. Using linear combinations of the three basis spectra, the resting, LLL-axial and LLL-rhombic signals, the experimental spectra were reconstructed as shown in Figures 1 and and2,2, and the proportions of each of the basis spectra used in the simulations of the experimental spectra are shown in Figure 3. Because the spectra contain both very broad and very sharp features, least-squares iterative fitting is not an appropriate fitting tool. The relative proportions of the resting and LLL-rhombic species were judged both by the overall fit to the spectrum (Figure 1) and by the fit of the complex hyperfine pattern at 700–1300 *G* (Figure 2), and changes in the values for the contributions of the resting and LLL-rhombic of more than 10% of those used for the simulations produced computed spectra that clearly did not match the experimental data. The simulations were relatively insensitive, however, to the inclusion of the LLL-axial species. Subtraction of traces A from traces B (Figure 1) clearly showed that the LLL-axial signal was present in trace B and integration of the simulation of the difference spectrum indicated that it accounted for ~10% of the spin density of the EPR signal after 10 ms. It is unclear whether an axial component is present in the spectrum of the resting enzyme or whether some residual contribution of an axial signal is present at 20 ms and beyond, but it is clear that the intensity of the LLL-axial signal increases up to 10 ms and diminishes thereafter. An interesting observation was that the spin Hamiltonian parameters of the much more well-defined LLL-rhombic species were very similar to those reported for the EPR signal observed upon the addition of the antitumour agent bestatin to [CoZn(VpAP)] [31] and, particularly, almost indistinguishable from those obtained [$S=^3/_2$, $M_S=|\pm½\rangle$, $g_{x,y}=2.55$, $g_z=2.40$, $D \gg g\beta BS$ (50 cm^{-1}), $E/D=0.28$ and $A_y^{I=7/2}(^{59}Co)=8.3\times10^{-3}$ cm^{-1}] from simulation of the signal elicited by the addition of amastatin to VpAP (Figure 4).

Biochemical Journal, Vol. 403, No. 3 (May 1, 2007): pg. 527-536. DOI.

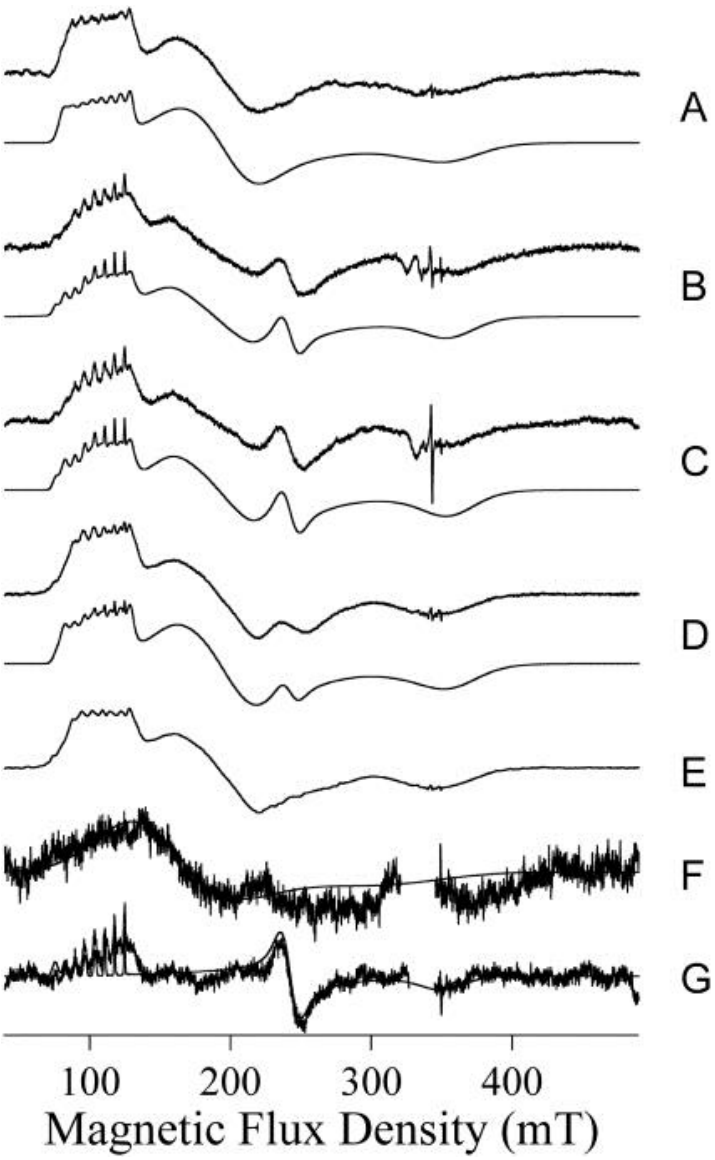

Figure 1: EPR spectra of VpAP upon reaction with LLL
Traces A–E show the experimental EPR signals (upper traces), and computer simulations thereof (lower traces), from resting [CoZn(VpAP)] (traces A), and VpAP upon reaction with LLL at 2 °C for 10 ms (traces B), 20 ms (traces C), 1 s (traces D) and 1 min (trace E). The experimental traces F and G were generated by difference and each is overlaid with a computer simulation; traces F are the LLL-axial EPR signal and traces G are the LLL-rhombic signal. The proportions of individual species, the resting, LLL-axial and LLL-rhombic, used for the simulations are indicated in Figure 3, and the spin Hamiltonian parameters for each are: resting, $S={}^3/_2$, $M_S=|\pm{}^1/_2\rangle$, $g_{x,y}=2.57$, $g_z=2.24$, $D \gg g\beta BS$ (50 cm^{-1}), $E/D=0.21$ and $A_y^{I=7/2}(^{59}Co)=8.1\times10^{-3}$ cm^{-1}; LLL-axial, $S={}^3/_2$, $M_S=|\pm{}^1/_2\rangle$, $g_{x,y}=2.28$, $g_z=2.20$, $D \gg g\beta BS$ (50 cm^{-1}) and $E/D=0.05$; LLL-rhombic, $S={}^3/_2$, $M_S=|\pm{}^1/_2\rangle$, $g_{x,y}=2.56$, $g_z=2.50$, $D \gg g\beta BS$ (50 cm^{-1}), $E/D=0.29$ and $A_y^{I=7/2}(^{59}Co)=8.4\times10^{-3}$ cm^{-1}.

Biochemical Journal, Vol. 403, No. 3 (May 1, 2007): pg. 527-536. DOI.

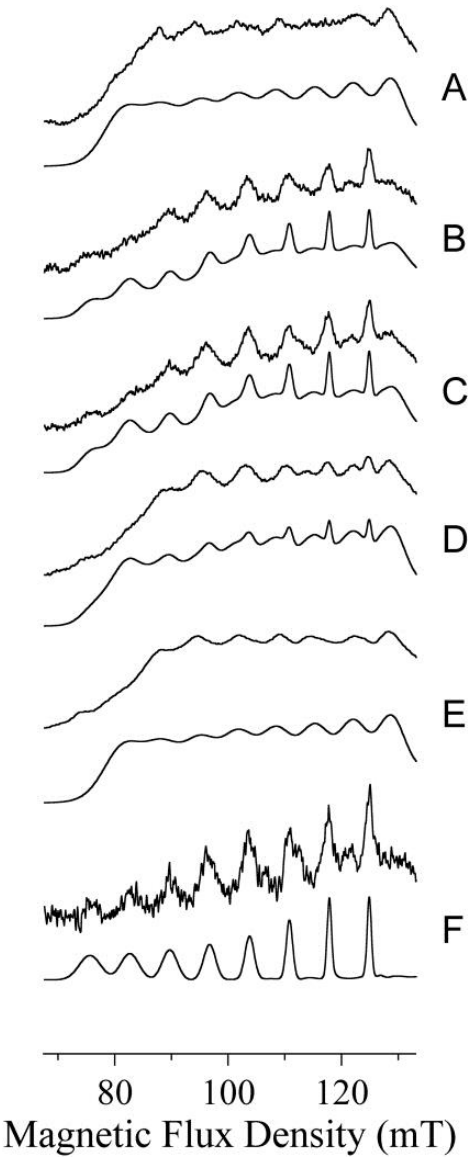

Figure 2: ^{59}Co hyperfine structure in the EPR spectra of VpAP upon reaction with LLL

Expanded region of the EPR spectra of resting [CoZn(VpAP)] (traces A), and of VpAP upon reaction with LLL at 2 °C for 10 ms (traces B), 20 ms (traces C) and 1 s (traces D) and 1 min (traces E); the upper traces of A–F are the experimental data and the lower traces are computer simulations. Trace F are of the LLL-rhombic species. The proportions of individual species, the resting, LLL-axial and LLL-rhombic, used for the simulations are indicated in Figure 3, and the spin Hamiltonian parameters for each are given in the legend to Figure 1.

Biochemical Journal, Vol. 403, No. 3 (May 1, 2007): pg. 527-536. DOI.

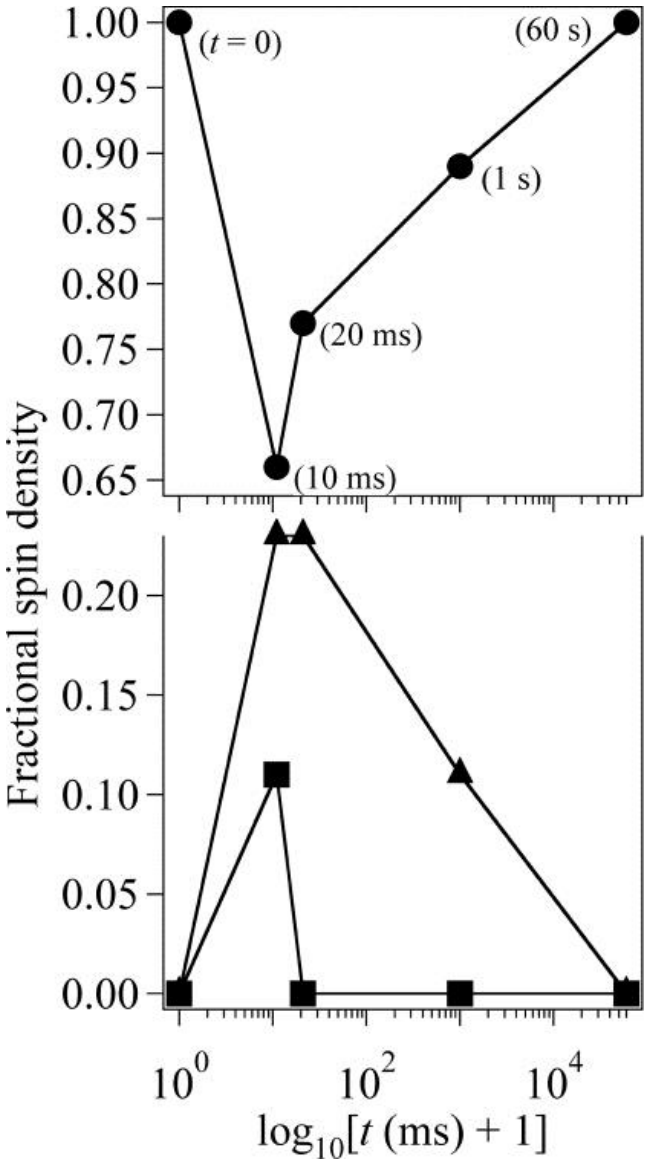

Figure 3: **Quantitative analysis of the EPR spectra of VpAP upon reaction with LLL**

Fractional intensities of the three EPR-detected species, the resting (●), LLL-axial (■) and LLL-rhombic (▲), of VpAP at rest and upon reaction with LLL for 10 ms, 20 ms, 1 s and 1 min.

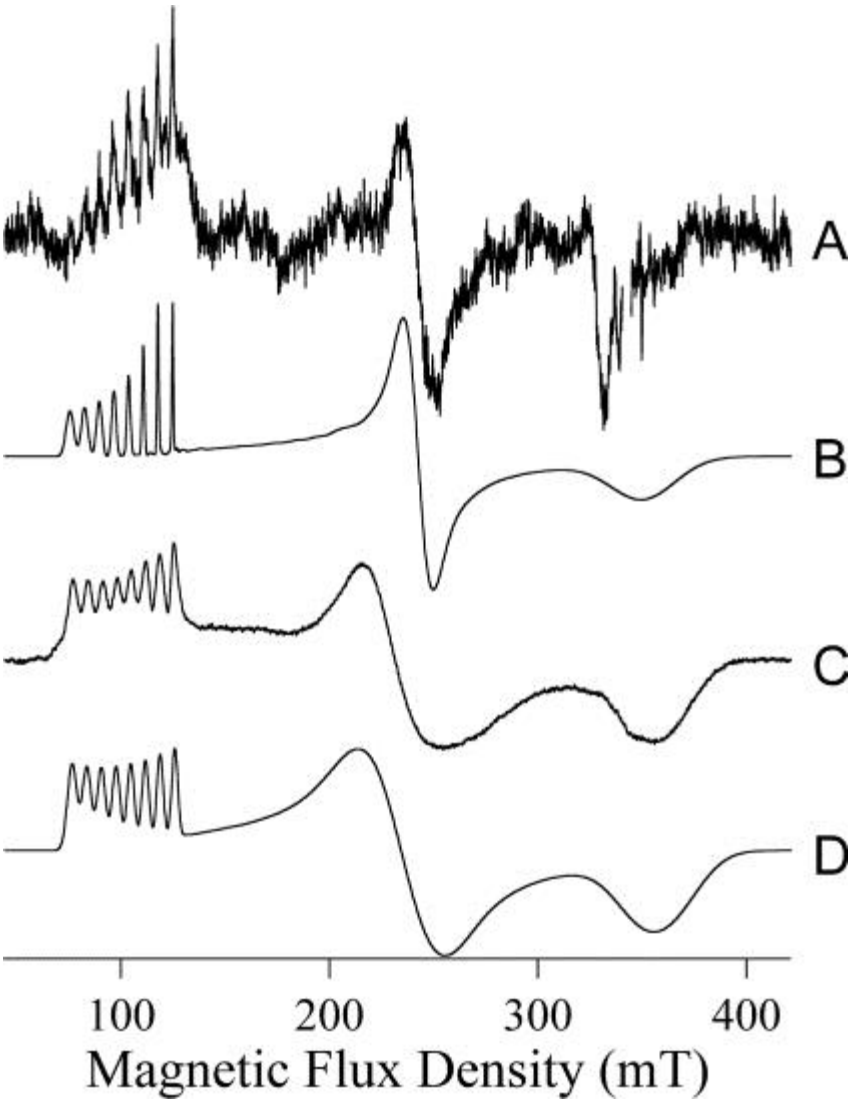

Figure 4: EPR spectra of complexes of [CoZn(VpAP)] with LLL and amastatin
Traces A and C are EPR spectra of the LLL-rhombic complex of [CoZn(VpAP)] with LLL (trace A) and of [CoZn(VpAP)] with amastatin (trace C). Traces B and D are computer simulations of A and C respectively. Trace B was generated using the spin Hamiltonian parameters $S={}^3/_2$, $M_S=|\pm{}^1/_2\rangle$, $g_{x,y}=2.56$, $g_z=2.50$, $D \gg g\beta BS$ (50 cm^{-1}), $E/D=0.29$ and $A_y^{I=7/2}(^{59}Co)=8.4\times10^{-3}$ cm^{-1}. Parameters for trace D were $S={}^3/_2$, $M_S=|\pm{}^1/_2\rangle$, $g_{x,y}=2.55$, $g_z=2.40$, $D \gg g\beta BS$ (50 cm^{-1}), $E/D=0.28$ and $A_y^{I=7/2}(^{59}Co)=8.3\times10^{-3}$ cm^{-1}.

X-ray crystallography

Crystals of VpAP soaked with LLL were hexagonal, with a space group of $P6_122$, as with other crystals of VpAP, and with unit cell parameters closest to those of the VpAP–BuBA complex (Table 1). The

Biochemical Journal, Vol. 403, No. 3 (May 1, 2007): pg. 527-536. DOI.

X-ray crystal structure of LLL-soaked VpAP was determined to a resolution of 2.0 Å (1 Å=0.1 nm) and the crystallographic data collection and refinement statistics are given in Table 1. The protein fold was found to be very similar to that of the native enzyme (PDB code 1AMP [28]) and Cα superimposition gave an RMSD (root mean square deviation) of 0.3 Å. Careful examination of omit maps and B-factors suggested that the electron density may be best described as representing a mixture of species, including LLL and LL bound at the active site (Figure 5). Additional possible contributions may arise from binding of LL and leucine in the S_1, S_1' and S_2' sites; leucine is a poor, purely competitive, inhibitor of VpAP, and LL is also an inhibitor of LLL hydrolysis, although the mechanism is less clear. The main indicator of the possibility of multiple species is the poor occupancy and/or high B-factors for the side chains of Leu^{295} when refining assuming 100% LLL bound. Additional refinements were carried out with leucine, LL, LA (Leu-Ala) and LAL (Leu-Ala-Leu). In each case, the backbone structure and the positions of the atoms of the P_1-leucine, that is bound to the active-site metals, are superimposable to well within the resolution of the structure. A detailed examination of the structure of VpAP–LLL revealed a number of very interesting features, some of which are paralleled in the structures of inhibited complexes of VpAP: (i) in a significant proportion of the sample, LLL is bound to both metal ions in the active site and is intact; similarly, intact LL is also observed bound in a manner entirely analogous to LLL (Figures 5 and and6);6); (ii) the N-terminal carbonyl appears to be trigonal planar (sp^2) indicating that the LLL and LL complexes represent pre-transition state complexes; (iii) LLL is bound with the side chain of P_1-leucine apparently *cis* to P_1'-leucine (P_1 denotes the N-terminal residue and P_1', P_2'…P_n' denote subsequent residues of substrates; S_1, S_1'…S_n' are the complementary enzyme subsites [52]); (iv) the N-terminal carbonyl of LLL (and LL) provides a μ-bridging oxygen atom that binds both metal ions, distinct from the terminal binding of the substrate analogue inhibitor BuBA (PDB code 1CP6 [29]) and from the more complex bridge found with the transition state analogue inhibitor LPA (PDB code 1FT7 [30]), but analogous to that seen with bestatin (PDB code 1TXR [31]); (v) the M2 Zn(II) ion is also bound to the P_1 amide nitrogen atom, forming a ring structure that includes M2 and is similar to that observed with LPA; (vi) there is no evidence for a water- or hydroxy-derived oxygen bound to M1 or bridging M1 and M2; (vii) the side chain of Glu^{151}, a

Biochemical Journal, Vol. 403, No. 3 (May 1, 2007): pg. 527-536. DOI.

residue implicated in proton delivery [32], appears to be *cis* to that of Glu^{152}, which provides an oxygen ligand to Zn1; (viii) there is a water molecule hydrogen-bonded to the Zn(II)-binding oxygen atom, OE1, of Glu^{152} [$r_{O(water)-OE1(Glu^{152})}$=2.7 Å; $r_{O(water)-Zn1}$=3.9 Å], analogous to that observed at 2.9 Å from Glu^{152} OE1 in the structure with bestatin. OE1 of Glu^{151} is hydrogen-bonded (2.8 Å) to the amide group of the P_1'-leucine of LLL (or LL). It should be noted that, in the cases of P_1-leucine and P_1'-leucine of LLL, and of Glu^{151} and Glu^{152} respectively, the apparent *cis* configuration of the side chains is not due to a *cis* peptide bond; this is evident in the case of LLL by examination along the peptide bond of the structure. Rather, rotation around the ψ_1 carbonyl-C–Cα bond of P_1-leucine of LLL, and the analogous C–Cα ψ bond of Glu^{151}, is responsible. Unlike in the case of a genuine *cis* pair, the appropriate residues fall into the additionally allowed category in the Ramachandran plot rather than the generously allowed category; we refer herein to such pairs of residues as adopting a 'torqued-ψ' configuration. Other features of this structure include the retention of the *cis* configuration, seen in the native structure, of Asp^{118} and the adjacent metal-bridging residue Asp^{117}. Asp^{118} was one of two residues in the generously allowed region of the Ramachandran plot, the other being the substrate-binding hydrophobic pocket residue Met^{180}. A water molecule is observed at 2.4 Å from the OD1 oxygen atom of Asp^{118}. The final significant difference between the native and LLL-bound structures is the conformation of the side chain of His^{105}; in the VpAP–LLL complex, this appears to fold over to form a 'cap' over the side chain of the P_2'-leucine of LLL, although no direct contact of His^{105} to LLL is made.

Biochemical Journal, Vol. 403, No. 3 (May 1, 2007): pg. 527-536. DOI.

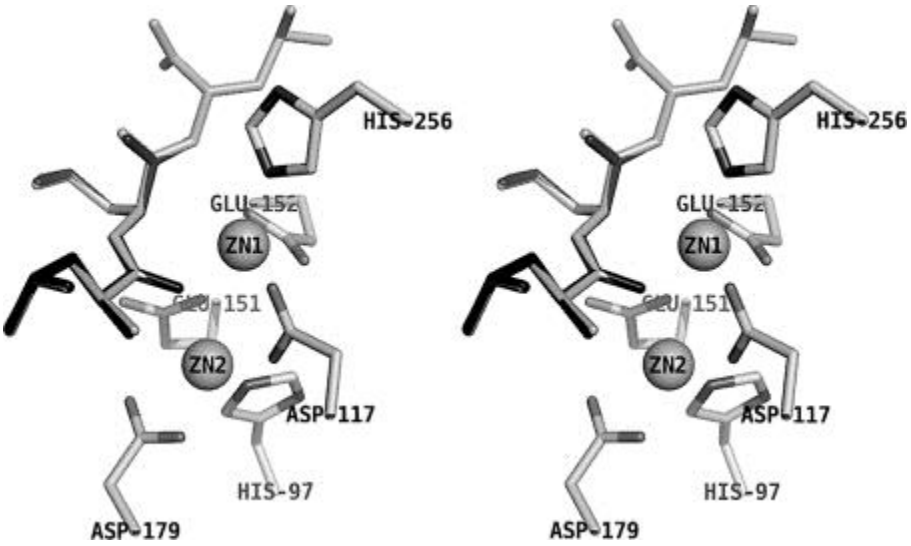

Figure 5: Active-site structure of crystalline VpAP soaked in LLL
Labels identify the two Zn(II) ions and the VpAP residues His^{97}, Asp^{117}, Glu^{151}, Glu^{152}, Asp^{179} and His^{256} of VpAP. The ligand is shown as an overlay of refined positions for leucine (black), LL (dark grey) and LLL (light grey) and the darkness reflects the occupancies.

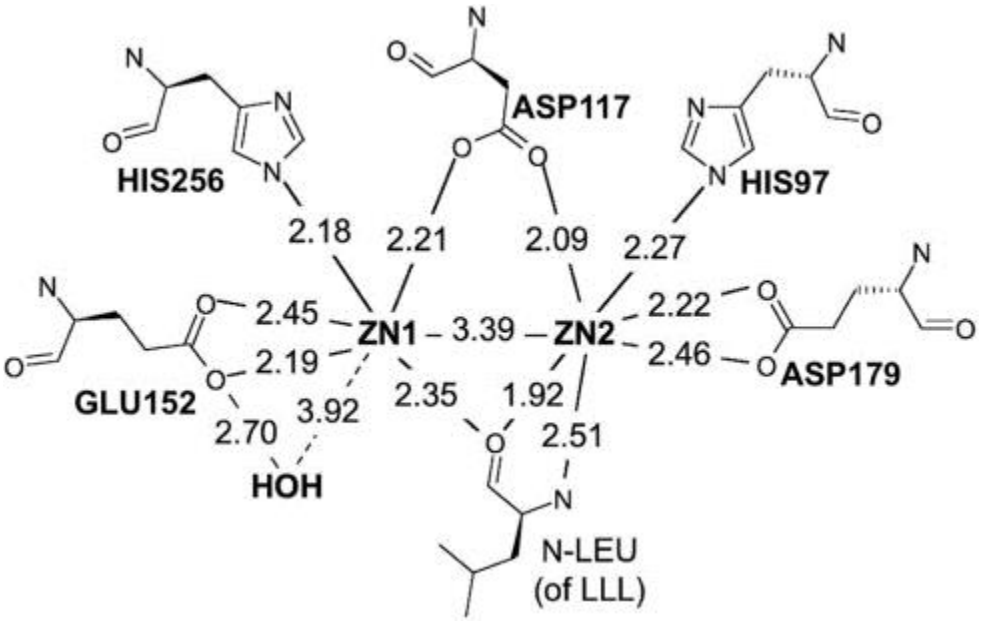

Figure 6: **Schematic diagram of the active site in the VpAP–LLL complex**
Interatomic distances are shown in Å.

Biochemical Journal, Vol. 403, No. 3 (May 1, 2007): pg. 527-536. DOI.

Parameter	Value
Unit cell parameters	
a (Å)	108.4
b (Å)	108.4
c (Å)	96.8
α, β, γ (°)	90, 90, 120
Collection and refinement parameters	
Total number of reflections	524877
Unique reflections	23236
Space group	$P6_122$
Resolution range (Å)	50.0–2.0
Last shell (Å)	2.07–2.00
R_{sym}	0.087
Overall completeness (%)	96.2
Last shell completeness (%)	78.3
R_{cryst}	0.206
R_{free}	0.247
Ramachandran plot	
Most favoured (%)	84.9
Additional allowed (%)	14.3
Generously allowed (%)	0.8 (Asp^{118}, Met^{180})
$<I/\sigma I>$	12.3

Table 1: Unit cell, symmetry and refinement parameters from crystallographic analysis of the VpAP–LLL complex (PDB code 2IQ6)

Discussion

RFQ–EPR is one of the few techniques that allow interrogation of catalytic intermediates in enzymatic reactions. In the present study, two intermediates have been shown by RFQ–EPR to be catalytically competent and one, the LLL-rhombic species, has been well characterized in terms of detailed spin Hamiltonian parameters. These parameters indicate a high degree of electronic structural similarity to the inhibited complexes of VpAP with bestatin and amastatin; analogous structural elements for these species are predicted. In particular, from both the EPR parameters of the LLL-rhombic species itself and by analogy with the EPR and structures of the bestatin and amastatin complexes of VpAP, the LLL-rhombic species is likely to involve multiple ligands to the dinuclear metal centre, including a metal-bridging oxygen, and does not accommodate an M1-bound water/hydroxy nucleophile candidate.

Biochemical Journal, Vol. 403, No. 3 (May 1, 2007): pg. 527-536. DOI.

The crystal structure of the VpAP–LLL complex is the first example of a structure of a leucine aminopeptidase complex with a *bona fide* substrate. This structure is highly analogous to that of the bestatin complex and the spectrokinetic RFQ–EPR data provide very strong evidence that the structure of the active site in the crystallographically characterized VpAP–LLL complex corresponds to the kinetically competent LLL-rhombic catalytic intermediate species in solution. Thus the crystallographic data provide high-resolution structural information on a species that has been determined to be a catalytically competent reaction intermediate in solution.

The crystal structure of the VpAP–LLL complex is extremely interesting in a number of respects. Most strikingly, the structure shows that LLL, or its primary product LL, is bound at the active site forming a pre-transition state complex, but that there is no water or hydroxy group bound to Zn1. LLL/LL provides one ligand, the μ-bridging carbonyl oxygen atom, to Zn1. Thus the co-ordination number of Zn1 in the VpAP–LLL complex and in the resting enzyme is the same. As the complex is a pre-transition state complex, formation of the transition state requires nucleophilic attack by a hydroxy group on the sp^2-hybridized carbonyl carbon atom to form a tetrahedral intermediate. In the previously proposed mechanism [29,30], the nucleophilic hydroxy group was proposed to arise as a result of terminalization on to Zn1 of a hitherto μ-bridging water or hydroxy group. This Zn1-bound hydroxy group, activated by the Lewis acidity of the Zn(II) ion, was then proposed to attack the substrate, also bound to Zn1. However, whereas there is evidence in a related methionyl aminopeptidase for a metal ion bound simultaneously to a substrate analogue and a nucleophilic hydroxy group [53], there is no such evidence for VpAP. The structure of the VpAP complex with the substrate analogue BuBA shows that the oxygen that was presumed to be that of the active nucleophile is weakly associated with the boron atom of BuBA (r_{B-O}=2.4 Å), but is completely dissociated from the Zn(II) ions. In other crystal structures of VpAP complexes, with bestatin and with LPA, there is also no M1-bound water molecule, but there is a water molecule hydrogen-bonded to OE2 of Glu^{152} in the LPA complex and to OE1 of Glu^{152} in the bestatin complex. The possible catalytic significance of this water molecule has been hitherto overlooked. The observation that there is no M1-bound water molecule, but that there is a water molecule hydrogen-bonded to

Biochemical Journal, Vol. 403, No. 3 (May 1, 2007): pg. 527-536. DOI.

Glu^{152} OE1 in the VpAP–LLL complex, however, takes on mechanistic significance if this species corresponds to a kinetically competent catalytic intermediate in solution. The perhaps startling implication is that the nucleophilic hydroxy group is activated and delivered to the substrate not from the catalytically essential M1 metal ion, but from either Glu^{152} or Asp^{118}. Glu^{152} is the most likely candidate, particularly given the inductive effect on Lewis acidity by virtue of also binding Zn(II), and initial work on site-directed variants has shown the catalytic importance of a carboxy-containing amino acid at position 152; a fuller characterization of Glu^{152} and Asp^{118} substitution variants is warranted. The delivery of the nucleophile by a carboxy group is a mechanistic aspect that is analogous to nucleophile activation by aspartate carboxy side chains in the aspartic proteases. A recent computational study led Guo and co-workers to propose that the nucleophile is not delivered by the metal ion in the class B2 metallo-β-lactamases, but, rather, by an aspartate residue [39]; this mechanism has distinct energetic benefits, and roles of the metal ion include electrophilic activation of substrate and stabilization of the leaving group. Activation of substrate by active-site metal ions, rather than nucleophile delivery, is a feature of the mechanism of class II aldolases [54].

The proposal that the active nucleophile in VpAP-catalysed hydrolysis is delivered not by a metal ion but by an active-site amino acid is supported by a wealth of circumstantial evidence. A number of observations are not well explained by the earlier proposed mechanism, but are much more consistent with the new one. First, VpAP exhibits substrate and reaction specificity, yet the active site is very exposed to the solvent. Active sites of the type found in VpAP are widely distributed among metallohydrolases, and a role in activating a nucleophilic hydroxy group would be unlikely to confer either reaction or substrate specificity. In VpAP, there is a hydrophobic patch adjacent to the active site and this probably plays a role in substrate recognition and specificity. However, with an exposed active site and an adjacent extended hydrophobic patch, it would be expected that VpAP would exhibit more stringent substrate specificity for larger substrates. In fact, precisely the opposite is observed. The substrate specificity of VpAP is most stringent for amino acid amides and amino acid *p*-nitroanilides, efficiently hydrolysing only the leucine, isoleucine, valine, methionine and phenylalanine derivatives. Substrate specificity is

Biochemical Journal, Vol. 403, No. 3 (May 1, 2007): pg. 527-536. DOI.

progressively less stringent for dipeptides and tripeptides, and only N-terminal aspartate, glutamate or cysteine are absolutely resistant to hydrolysis in some larger peptides [36,37]. The key to understanding the substrate specificity may be in appreciating the significance of the finding that the P_1- and P_1'-leucine residues in the VpAP–LLL complex are in a torqued-ψ configuration. This configuration is stabilized by the interaction of the P_1-leucine amino nitrogen with Zn2, and the proximity of the P_1 and P_1' side chains results in sterically induced strain in the peptide bond. The relevance of this to catalysis is highlighted by the high enthalpy of hydrolysis by VpAP, indicative of conformational change. It is proposed here that the role of the metal ions is therefore to act in concert with the hydrophobic patch to induce the P_1-P_1' torqued-ψ conformation change and stabilize the consequent pre-transition state complex, weakening the scissile bond for hydrolysis. Furthermore, binding to the metal ions electrophilically activates the carbonyl carbon atom for nucleophilic attack. A torqued-ψ conformation is of little consequence for amino acid amides and *p*-nitroanilides, and only the most favourable bulky hydrophobic substrates are hydrolysed efficiently. Dipeptides are the smallest substrates that can be geometrically activated via an enzyme-induced torqued-ψ conformation. This higher energy conformation can be stabilized further by interaction of larger substrates with the hydrophobic patch, particularly those with hydrophobic P_1', P_2' etc. residues; the phenomenon is reflected in the more efficient and less N-terminal-specific hydrolysis of peptides with hydrophobic P_1', P_2' and P_3' residues [35,37].

Other observations perhaps further the contention that the role of the metal centre, and M1 in particular, is not to activate and deliver the nucleophile to the substrate. First, the pH-dependence of k_{cat} indicated that the free base form of an enzyme functional group with pK_a of ~5.3 is required for hydrolysis of bound substrate [55]. This suggests that the nucleophile is either derived from an aspartyl or glutamyl carboxy group; more specifically, work on thermolysin has suggested a concerted 'inductive' effect of a Glu-COO^--H_2O-Zn(II) structure in deprotonation of the carboxylate hydroxy group [56] and therefore supports the hypothesis that the nucleophile is bound to the same carboxy group oxygen, OE1 of Glu^{152}, that is bound to Zn1 in the VpAP–LLL complex. A second observation on VpAP that is not well-explained by the earlier proposed mechanism is the complex pattern of

activation of apoVpAP by transition metal ions. VpAP can be activated with Zn(II), Co(II), Ni(II) and Cu(II), and the degree of activation of the enzyme is dependent both upon the chemical identity of the metal ions added and their order of addition, but not with Fe(II) or Mn(II) [26,38]. The activation observed is not predictable on the basis of the Lewis acidity of M1. For instance, [ZnCu(VpAP)] is as active as the monometallic [Zn_(VpAP)] and is 80% as active as the homodimetallic [ZnZn(VpAP)], whereas [Cu_(VpAP)] and [CuCu(VpAP)] are 5–6-fold more active than [ZnZn(VpAP)]; [CuZn(VpAP)], on the other hand, is two orders of magnitude more active than [ZnZn(VpAP)], and Ni(II) elicits an activation profile analogous to that of Cu(II). The ability of Cu(II) at the M1 site to activate VpAP, but not the related methionyl aminopeptidase has been proposed to indicate that specificity is dependent upon the co-ordination geometry of the M1 ion rather than Lewis acidity [57]. The pronounced hyperactivity of [CuZn(VpAP)] over [CuCu(VpAP)] indicated that the precise structure of the dinuclear site is important; Cu2 in [CuCu(VpAP)] is not bound in the same site as Zn in [CuZn(VpAP)]. The apparent requirement for nucleophile activation with a pK_a of ~5.3 and the sensitivity of VpAP activity to the active-site geometry are entirely consistent with a Glu^{152}-derived nucleophile and a role for the metal ions in substrate binding and activation rather than of nucleophile activation. The torqued-ψ arrangement of Glu^{151} and Glu^{152}, and the role of Glu^{151} in proton transfer to the substrate [32], provide further circumstantial support for the role of Glu^{152}. The observation that Asp^{117} and Asp^{118}, and Glu^{151} and Glu^{152}, are in *cis* and torqued-ψ configurations respectively, was made in the original report of the crystal structure of VpAP, and the general phenomenon that non-proline *cis* amino acid pairs are generally involved in catalysis was noted and discussed [28].

The new proposal, that the nucleophile in VpAP-catalysed hydrolysis is not delivered by the metal ion, is consistent with all the earlier reported data on VpAP and with the crystal structure described herein, and it better explains other phenomena observed with VpAP. This circumstantial evidence supports the new mechanism and therefore the contention that the crystallographically characterized active site in the VpAP–LLL complex corresponds to a genuine catalytic intermediate. Experimental evidence for this contention is, however, very desirable and would considerably strengthen the case for the new mechanism. EPR studies supply this crucial evidence. Co(II) in the M1

Biochemical Journal, Vol. 403, No. 3 (May 1, 2007): pg. 527-536. DOI.

position of [CoZn(VpAP)] exhibits a rhombic EPR signal with resolved hyperfine structure and, along with electronic absorption spectrophotometry, these data indicate a five-co-ordinate site with a relatively constrained and distorted geometry that includes a μ-bridging hydroxy group as a ligand to Co(II) [1,25,26]. Upon reaction of [CoZn(VpAP)] with LLL under reaction conditions where the turnover time is 380 ms, two new EPR species are detected, with significant yields, within 10 ms. The first, the LLL-axial species, is indicative of a six-co-ordinate Co(II) species with axial electronic symmetry and a free water or hydroxy group ligand that is responsible for the microheterogeneous structure of the Co(II) ions, reflected in the very broad EPR signal [1]. This species accounts for approx. 10% of the enzyme molecules and rapidly diminishes thereafter; it is therefore short-lived. The second species, the LLL-rhombic species, is a five-co-ordinate species that is clearly distinct, both by observation and from the spin Hamiltonian parameters, from the resting species. The very narrow linewidths indicate that the co-ordination sphere consists of 'rigid' ligands with very little geometrical heterogeneity among the population and argues strongly against co-ordinated water or hydroxy group. Furthermore, this signal is very similar to the signals elicited by amastatin and bestatin. The LLL-rhombic species accounts for 23% of the enzyme molecules during the pre-steady-state phase of the first turnover and diminishes to 11% by the third turnover. The high pre-steady-state concentrations of this species and the lower concentrations as conditions approach the steady state are characteristic of a relatively long-lived, but nevertheless catalytically competent, intermediate that is formed after the LLL-axial species. Thus EPR indicates that, upon reaction of the five-co-ordinate, hydroxy group-bearing Co(II) ion in [CoZn(VpAP)] with LLL, the six-co-ordinate LLL-axial species, bearing an unconstrained water or hydroxy group, is first formed. This is presumably due to substrate binding via the carbonyl oxygen. However, rather than this step being followed by nucleophilic attack, a subsequent five-co-ordinate intermediate species devoid of a free water/hydroxy group ligand, the LLL-rhombic, is formed instead. Thus, consistent with the new mechanism, RFQ–EPR identifies two kinetically competent catalytic intermediates: the first formed by addition of substrate and the second by subsequent dissociation of a water or hydroxy group.

Biochemical Journal, Vol. 403, No. 3 (May 1, 2007): pg. 527-536. DOI.

A central question is whether either of the EPR-identified intermediates correspond to the crystallographically characterized active site in VpAP–LLL. The structure of the bestatin and amastatin complexes of VpAP is well-characterized, and the active site in these complexes is very similar indeed to that of the VpAP–LLL complex described herein, including a ligand carbonyl-derived μ-oxygen bridge, an LLL-derived ring structure based on M2, the lack of an M1-bound candidate for the nucleophile and the presence of a water molecule hydrogen-bonded to OE1 of Glu^{152}. It is therefore most striking that this structural similarity is paralleled by the congruency of the EPR signals of the bestatin and amastatin species with that of the LLL-rhombic signal observed in RFQ–EPR experiments on VpAP with LLL. It is also remarkable that the details of the EPR spectrum of the LLL-rhombic species are entirely consistent with the structure of the VpAP–LLL complex. The likely conclusion, then, is that the crystallographically characterized active site of VpAP–LLL corresponds to a kinetically competent catalytic intermediate, the LLL-rhombic species, of the reaction of VpAP with LLL. These data provide very solid support for the newly proposed mechanism.

A final phenomenon worthy of discussion is the low catalytic activity of crystalline VpAP towards LLL. The crystallographic data suggest that some activity had occurred, as LL is seen binding as a substrate in an analogous manner to LLL. Furthermore, it is likely that LL was partially hydrolysed and a number of species in which leucine is bound to VpAP may be present. It is noteworthy that leucine is a pure competitive inhibitor of VpAP and that, even at very high concentrations, does not bind to Co(II) in cobalt-substituted VpAP. Nevertheless, the high concentrations of leucine and LL may have contributed to the poor activity of VpAP towards LLL, perhaps via an entropic mechanism. Another possible reason for the low activity of crystalline VpAP towards LLL (and LL) is that a conformational change is required, as indicated by thermodynamic analyses, that is inhibited in the crystalline state. The change in crystal appearance upon soaking with LLL and the increased fragility of the crystals may suggest this. As the protein fold is identical in VpAP–LLL and native (or Tris-complexed) VpAP, this may suggest that a conformational change occurs after substrate binding and reorientation. A second possibility is that while the active site of VpAP–LLL corresponds to that in the reaction intermediate, the protein fold differs in solution from that in the

Biochemical Journal, Vol. 403, No. 3 (May 1, 2007): pg. 527-536. DOI.

crystal. Finally, the altered conformation of the side-chain His^{105} may or may not be significant. EPR spin-labelling experiments are underway to address some of these issues.

In summary, very strong evidence is presented that the active nucleophile in VpAP catalysis is not delivered by the metal centre. The most likely candidate for the nucleophile is a water molecule hydrogen-bonded to a carboxylate oxygen atom, itself a ligand to a Zn(II) ion, of an active-site glutamate residue, Glu^{152}. These findings prompt a theoretical revisiting of the mechanisms of metallohydrolases and have significant consequences for rational design of therapeutically important inhibitors of these enzymes.

Acknowledgments

We thank Thomas Rummel and Derek Francis for preliminary RFQ studies, Jason Kowalski for assistance with the RFQ studies herein, Richard C. Holz for providing the *V. proteolyticus* culture, for helpful discussions and for providing information prior to publication, Andrea Funk for superb technical assistance, and Michael W. Crowder for careful reading of this work at an early stage and for numerous helpful discussions. This work was supported by the National Institutes of Health (NIAID R01 AI056231 to B. B.) and EPR instrumentation was supported in part by the National Biomedical EPR Center (NIH NIBIB P41 EB001980 to James S. Hyde).

References

1. Bennett B. EPR of Co(II) as a structural and mechanistic probe of metalloprotein active sites: characterisation of an aminopeptidase. *Curr. Top. Biophys*. 2002;26:49–57.
2. Barrett A. J., Rawlings N. D. (eds) London: Elsevier Academic Press; 1998. *Handbook of Proteolytic Enzymes*.
3. Arfin S. M., Bradshaw R. A. Cotranslational processing and protein turnover in eukaryotic cells. *Biochemistry*. 1988;27:7979–7984.
4. Bradshaw R. A. Protein translocation and turnover in eukaryotic cells. *Trends Biochem. Sci*. 1988;14:276.
5. Arechaga G., Martinez J. M., Prieto I., Ramirez M. J., Alba F., Ramirez M. Changes in membrane-bound leucine aminopeptidase activity during maturation and ageing of brain. *Biochem. Mol. Biol. Int*. 1999;47:861–868.
6. Taylor A., Daims M., Lee J., Surgenor T. Identification and quantification of leucine aminopeptidase in aged normal and cataractous human lenses

and ability of bovine lens LAP to cleave bovine crystallins. *Curr. Eye Res*. 1982;2:47–56.

7. Pulido-Cejudo G., Conway B., Proulx P., Brown R., Izaguirre C. A. Bestatin-mediated inhibition of leucine aminopeptidase may hinder HIV infection. *Antivir. Res*. 1997;36:167–177.
8. Scoglio M. E., DiPietro A., Picerno I., Delia S., Mauro A., Lagana P. Virulence factors in Vibrios and Aeromonads isolated from seafood. *New Microbiol*. 2001;24:273–280.
9. Hashida H., Takabayashi A., Kanai M., Adachi M., Kondo K., Kohno N., Yamaoka Y., Miyake M. Aminopeptidase N is involved in cell motility and angiogenesis: its clinical significance in human colon cancer. *Gastroenterology*. 2002;122:376–386.
10. Zhang P., Nicholson D. E., Bujnicki J. M., Su X., Brendle J. J., Ferdig M., Kyle D. E., Milhous W. K., Chiang P. K. Angiogenesis inhibitors specific for methionine aminopeptidase 2 as drugs for malaria and leishmaniasis. *J. Biomed. Sci*. 2002;9:34–40.
11. Ishii K., Usui S., Sugimura Y., Yoshida S., Hioki T., Tatematsu M., Yamamoto H., Hirano K. Aminopeptidase N regulated by zinc in human prostate participates in tumor cell invasion. *Int. J. Cancer*. 2001;92:49–54.
12. Kaznowski A., Wlodarczak K. Enzymatic characterization of Vibrionaceae strains isolated from environment and cold-blooded animals. *Acta Microbiol. Pol.* 1991;40:71–76.
13. Maras B., Greenblatt H. M., Shoham G., Spungin-Bialik A., Blumberg S., Barra D. Aminopeptidase from *Streptomyces griseus*: primary structure and comparison with other zinc-containing aminopeptidases. *Eur. J. Biochem*. 1997;236:843–846.
14. Centers for Disease Control (CDC) *Aeromonas* wound infections associated with outdoor octivities: California. *MMWR Morb. Mortal. Wkly. Rep.* 1990;39:334–335.
15. Centers for Disease Control Prevention (CDC) Outbreak of *Vibrio parahaemolyticus* infections associated with eating raw oysters: Pacific Northwest, 1997. *MMWR Morb. Mortal. Wkly. Rep*. 1998;47:457–462.
16. Centres for Disease Control Prevention (CDC) Outbreak of *Vibrio parahaemolyticus* infection associated with eating raw oysters and clams harvested from Long Island Sound: Connecticut, New Jersey and New York, 1998. *MMWR Morb. Mortal. Wkly. Rep*. 1999;48:48–51.
17. Yadav A. S., Kumar A. Prevalence of enterotoxigenic motile aeromonads in children, fish, milk and ice-cream and their public health significance. *Southeast Asian J. Trop. Med. Public Health*. 2000;31(Suppl. 1):153–156.
18. Benassi F. O., Vergara M., von Specht M. H., Garcia M. A., Quiroga M. I., Pucciarelli A. B., Zubreski E., Laczeski M., Martin B. M., Leardini N.,

Gutkind G. β-Lactam antibiotic sensitivity in *Aeromonas* spp. of clinical, animal and environmental origin. *Rev. Argent. Microbiol*. 2001;33:47–51.

19. Hansen L. T., Austin J. W., Gill T. A. Antibacterial effect of protamine in combination with EDTA and refrigeration. *Int. J. Food Microbiol*. 2001;66:149–161.
20. Fujii H., Nakajima M., Aoyagi T., Tsuruo T. Inhibition of tumor cell invasion and matrix degradation by aminopeptidase inhibitor. *Biol. Pharm. Bull.* 1996;19:6–10.
21. Jones D. T. GenTHREADER: An efficient and reliable protein fold recognition method for genomic sequences. *J. Mol. Biol*. 1999;287:797–815.
22. Davis M. I., Bennett M. J., Thomas L. M., Bjorkman P. J. Crystal structure of prostate-specific membrane antigen, a tumor marker and peptidase. *Proc. Natl. Acad. Sci. U.S.A*. 2005;102:5981–5986.
23. Chevrier B., Schalk C., D'Orchymont H., Rondeau J.-M., Moras D., Tarnus C. Crystal structure of *Aeromonas proteolytica* aminopeptidase: a prototypical member of the co-catalytic zinc enzyme family. *Structure*. 1994;2:283–291.
24. Bennett B., Holz R. C. EPR studies on the mono- and dicobalt(II)-substituted forms of the aminopeptidase from *Aeromonas proteolytica*: insight into the catalytic mechanism of dinuclear hydrolases. J*. Am. Chem. Soc.* 1997;119:1923–1933.
25. Bennett B., Holz R. C. Spectroscopically distinct cobalt(II) sites in heterodimetallic forms of the aminopeptidase from *Aeromonas proteolytica*: characterization of substrate binding. *Biochemistry*. 1997;36:9837–9846.
26. Prescott J. M., Wagner F. W., Holmquist B., Vallee B. L. Spectral and kinetic studies of metal-substituted *Aeromonas* aminopeptidase: nonidentical, interacting metal-binding sites. *Biochemistry*. 1985;24:5350–5356.
27. Bennett B., Holz R. C. Inhibition of the aminopeptidase from *Aeromonas proteolytica* by L-leucinephosphonic acid, a transition state analogue of peptide hydrolysis. *J. Am. Chem. Soc.* 1998;120:12139–12140.
28. Chevrier B., D'Orchymont H., Schalk C., Tarnus C., Moras D. The structure of the *Aeromonas proteolytica* aminopeptidase complexed with a hydroxamate inhibitor: involvement in catalysis of Glu^{151} and two zinc ions of the cocatalytic unit. *Eur. J. Biochem*. 1996;237:393–398.
29. DePaola C., Bennett B., Holz R. C., Ringe D., Petsko G. L-Butaneboronic acid binding to *Aeromonas proteolytica* aminopeptidase: a case of arrested development. *Biochemistry*. 1999;38:9048–9053.

Biochemical Journal, Vol. 403, No. 3 (May 1, 2007): pg. 527-536. DOI.

30. Stamper C., Bennett B., Edwards T., Holz R. C., Ringe D., Petsko G. Inhibition of the aminopeptidase from *Aeromonas proteolytica* by L-leucinephosphonic acid: spectroscopic and crystallographic characterization of the transition state of peptide hydrolysis. *Biochemistry*. 2001;40:7035–7036.
31. Stamper C. C., Bienvenue D. L., Bennett B., Ringe D., Petsko G., Holz R. C. Spectroscopic and X-ray crystallographic characterization of bestatin bound to the aminopeptidase from *Aeromonas* (*Vibrio*) *proteolytica*. *Biochemistry*. 2004;43:9620–9628.
32. Bzymek K. P., Holz R. C. The catalytic role of glutamate 151 in the leucine aminopeptidase from *Aeromonas proteolytica*. *J. Biol. Chem*. 2004;279:31018–31025.
33. Bayliss M. E., Prescott J. M. Modified activity of *Aeromonas* aminopeptidase: metal ion substitution and role of substrates. *Biochemistry*. 1986;25:8113–8117.
34. Bayliss M. E., Wilkes S. H., Prescott J. M. *Aeromonas* neutral protease: specificity toward extended substrates. *Arch. Biochem. Biophys.* 1980;204:214–219.
35. Izawa T., Ishikawa S., Tanokura T., Ohta K., Hayashi K. Purification and characterization of *Aeromonas caviae* aminopeptidase possessing debittering activity. *J. Agric. Food Chem*. 1997;45:4897–4902.
36. Wagner F. W., Wilkes S. H., Prescott J. M. Specificity of *Aeromonas* aminopeptidase towards amino acid amides and dipeptides. *J. Biol. Chem.* 1972;247:1208–1210.
37. Wilkes S. H., Bayliss M. E., Prescott J. M. Specificity of *Aeromonas* aminopeptidase towards oligopeptides and polypeptides. *Eur. J. Biochem*. 1973;34:159–166.
38. Prescott J. M., Wagner F. W., Holmquist B., Vallee B. L. One hundred fold increased activity of *Aeromonas* aminopeptidase by sequential substitutions with Ni(II) or Cu(II) followed by zinc. *Biochem. Biophys. Res. Commun.* 1983;114:646–652.
39. Xu D., Xie D., Guo H. Catalytic mechanism of class B2 metallo-β-lactamase. *J. Biol. Chem*. 2006;281:8740–8747.
40. Gill S. C., von Hippel P. H. Calculation of protein extinction coefficients from amino acid sequence data. *Anal. Biochem*. 1989;182:319–326.
41. Laemmli U. K. Cleavage of structural proteins during the assembly of the head of bacteriophage T4. Nature. 1970;227:680–685.
42. Bradford M. A rapid and sensitive method for the quantitation of microgram quantities of protein utilizing the principle of protein-dye binding. *Anal. Biochem*. 1976;72:248–254.
43. Bzymek K. P., D'Souza V. M., Chen G., Campbell H., Mitchell A., Holz R. C. Function of the signal peptide and N- and C-terminal propeptides

Biochemical Journal, Vol. 403, No. 3 (May 1, 2007): pg. 527-536. DOI.

in the leucine aminopeptidase from *Aeromonas proteolytica*. *Protein Expression Purif.* 2004;37:294–305.
44. Marangoni A. G. Enzyme Kinetics: A Modern Approach. Hoboken: John Wiley & Sons; 2003. *Characterization of enzyme activity*; pp. 44–60.
45. Garrity J. D., Bennett B., Crowder M. W. Direct evidence that the reaction intermediate of metallo-β-lactamase L1 is metal bound. *Biochemistry*. 2005;44:1078–1087.
46. Hanson G. R., Gates K. E., Noble C. J., Mitchell A., Benson S., Griffin M., Burrage K. XSophe-Sophe-XeprView: a computer simulation software suite for the analysis of continuous wave EPR spectra. In: Shiotani M., Lund A., editors. *EPR of Free Radicals in Solids: Trends in Methods and Applications.* Dordrecht: Kluwer Press; 2003. pp. 197–237.
47. Desmarais W., Bienvenue D. L., Bzymek K., Holz R. C., Petsko G., Ringe D. The 1.20 Å resolution crystal structure of the aminopeptidase from *Aeromonas proteolytica* complexed with Tris: a tale of buffer inhibition. *Structure*. 2002;10:1063–1072.
48. Otwinowski Z., Minor W. Processing of X-ray diffraction data collected in oscillation mode. *Methods Enzymol*. 1997;276:307–326.
49. Collaborative Computational Project Number 4. The CCP4 suite: programs for protein crystallography. *Acta Crystallogr. Sect. D Biol. Crystallogr*. 1994;50:760–763.
50. Brunger A. T., Adams P. D., Clore G. M., DeLano W. L., Gros P., Grosse-Kunstleve R. W., Jiang J. S., Kuszewski J., Nilges M., Pannu N. S., et al. Crystallography & NMR system: a new software suite for macromolecular structure determination. *Acta Crystallogr. Sect. D Biol. Crystallogr.* 1998;54:905–921.
51. Laskowski R. A., MacArthur M. W., Moss D. S., Thornton J. M. PROCHECK: a program to check the stereochemical quality of protein structures. *J. Appl. Crystallogr.* 1993;26:283–291.
52. Schechter I., Berger A. On the active site in proteases. I. Papain. *Biochem. Biophys. Res. Commun*. 1967;27:157–162.
53. Copik A. J., Waterson S., Swierczek S. I., Bennett B., Holz R. C. Both nucleophile and substrate bind to the catalytic Fe(II)-center in the type-II methionyl aminopeptidase from *Pyrococcus furiosus*. *Inorg. Chem.* 2005;44:1160–1162.
54. Horecker B. L., Tsolas O., Lai C. Y. Aldolases. In: Boyer P. D., editor. *The Enzymes*. New York: Academic Press; 1972. pp. 213–258.
55. Baker J. O., Prescott J. M. *Aeromonas* aminopeptidase: pH dependence and a transition-state-analogue inhibitor. *Biochemistry*. 1983;22:5322–5331.
56. Lipscomb W. N., Sträter N. Recent advances in zinc enzymology. *Chem. Rev.* 1996;96:2375–2433.

57. Bennett B., Antholine W. E., D'souza V. M., Chen G., Ustinyuk L., Holz R. C. Structurally distinct active sites in the copper(II)-substituted aminopeptidase from *Aeromonas proteolytica*. *J. Am. Chem. Soc*. 2002;124:13025–13034.